Influence of impurities on the phase transitions in chiral magnets: Monte Carlo calculations

A. M. Belemuk *
Institute for High Pressure Physics, Russian Academy of Science, Troitsk 108840, Russia

S. M. Stishov
P. N. Lebedev Physical Institute, Russian Academy of Sciences, Moscow 119991, Russia

(Received 22 March 2021; accepted 26 July 2021; published 4 August 2021)

Using classical Monte Carlo simulation we investigate the evolution of the specific heat in chiral magnets with impurities. Our calculations are made in the framework of a spin lattice model and could be applicable to an analysis of the specific heat in transition-metal monosilicides $Mn_{1-x}(Fe,Co)_xSi$ with increasing doping. We propose two tentative models for impurity positions in the lattice. In the first one, impurities substitute the regular transition-metal ions in a parent compound. The second one treats impurities as frozen spins placed into interstitial positions of the regular lattice and coupled with their nearest neighbors by random exchange interactions. In both models an increase of doping leads to a quick degradation of the magnetic phase transition, though an evolution of the hump anomaly is not similar. We provide a comparison of the behavior of the specific heat and Bragg scattering amplitude for these two models.

DOI: 10.1103/PhysRevB.104.064404

I. INTRODUCTION

One of the debating topics in the physics of the chiral helimagnets is the description of their magnetic phase transition which is characterized by an unusual behavior of a number of thermodynamic quantities. In particular, one sees the formation of the hump anomaly in the heat capacity, thermal expansion, and elastic moduli above the temperature of the magnetic phase transition [1–5]. This anomaly results from the strong spin fluctuations as is revealed by the small angle neutron scattering experiments [6–9]. The experiments indicate strong chiral fluctuations in scattering intensity at temperatures corresponding to the hump anomaly. In $\boldsymbol{k}$ space these fluctuations are localized in a spherical layer with a radius equal to a wave vector of the corresponding helix in the low-temperature spiral phase.

Another interesting aspect of the subject is the role of disorder and its effect on the magnetic phase transition in chiral magnets. Doping has different effects on the magnetic structure of MnSi and MnGe parent compounds. Doping MnGe by Fe shows continuous evolution of the spin helix wave vector from its maximum value for pure MnGe to zero value at $x_c \simeq 0.75$, and an increase to another maximum value for the pure FeGe [10]. Compound $Mn_{1-x}Fe_xGe$ is magnetically ordered in the whole range of concentrations. The opposite effect appears on doping MnSi; material $Mn_{1-x}Fe_xSi$ shows spin ordering only in a narrow interval of doping concentration $x \lesssim 0.17$, while pure FeSi is not magnetically ordered.

The detailed study of the evolution of the helimagnetic correlation in $Mn_{1-x}Fe_xSi$ with doping indicates [11,12] that the helimagnetic Bragg peaks disappear at doping concentration $x^* \sim 0.11$, while the magnetic transition temperature vanishes at a larger concentration $x_c \sim 0.17$. Concentration x^* corresponds to an abrupt disappearance of the long-range helimagnetic periodicity [11], and the range of composition between x^* and x_c corresponds to short-range helimagnetic correlations and is viewed as a consequence of a chiral spin liquid state [12]. An analysis of the behavior of thermodynamic quantities in $Mn_{1-x}Fe_xSi$ and $Mn_{1-x}Co_xSi$ [13–15] shows that impurities eliminate the signature of the first-order transition; they spread the fluctuation maximum of the specific heat in a such way that its low-temperature part presumably reaches zero temperature. This suggests that intensive helical fluctuations accompanying the magnetic transition in helimagnets over a significant range of doping concentrations at finite temperatures become quantum close to zero temperature [16,17].

Another important development in the field is the discovery of a spin-glass state in $Mn_{1-x}Co_xSi$ for Co concentrations $0.05 < x < 0.90$ [18]. This state is attributed to a formation of localized magnetic moments. Helimagnetic structure is conserved only in a concentration range below $x = 0.04$; above the critical concentration $x_c = 0.06$ the compound $Mn_{1-x}Co_xSi$ does not show any magnetic order [18]. In recent measurements, however, the formation of a spin-glass state for Co concentrations lower than $x = 0.5$ was questioned [15]. The discrepancy probably originates from an inaccurate calculation of the impurity concentration after annealing in [18].

In the present study we investigate helimagnetic correlations and the thermodynamic response in a chiral helimagnet with transition-metal impurities; the main application of our model we have in mind is Fe or Co doping to the itinerant helimagnet MnSi. For the parent helimagnet we use a classical model of unit spins placed onto sites of the regular lattice which are coupled by exchange and Dzyaloshinskii-Moriya

*abel@hppi.troitsk.ru

(DM) interactions. We propose two models to take into account the doped atoms. In the first model we assume that an impurity replaces a regular Mn ion in the parent compound. In terms of the spin lattice model it amounts to a substitution of an impurity spin in place of a regular spin. Such a substitution would naturally modify the exchange and DM coupling constants of the impurity spin with its neighbors.

In the second model we add impurities into interstitial positions of the lattice and treat the dopant as a frozen spin. For each frozen spin we set random exchange couplings with nearest spins of the regular lattice. Such an arrangement of impurities is probably more relevant for an experiment when one knows only the amount of the dissolved impurities but does not know exactly where they reside in the lattice. We believe that these two phenomenological arrangements of impurities are relevant for low impurity concentrations far from quantum criticality and allows one to partly explain to what extent the classical model of spin-spin interaction can capture the physics of helimagnets upon doping.

We use a classical Monte Carlo (MC) simulation technique to investigate the thermodynamic response of the system upon doping. We compare the evolution of the specific heat and the corresponding spin structures of both models, and find that the main signature of the unusual temperature behavior of the specific heat, namely, the hump anomaly, persists with doping. Upon doping helimagnetic correlations reveal themselves in a similar way as for the parent MnSi, namely, the ring-shape structure of the Bragg intensity profile is seen in a temperature range above that of the magnetic transition temperature. However, the evolution of the hump profile is different in the proposed models.

II. MODEL

For the parent helimagnet we use the lattice spin model [19–24], which treats spin variables as classical unit vectors coupled by exchange and DM spin-spin interactions. The Hamiltonian of the model reads

$$H_{\rm lat} = -\sum_{\boldsymbol{r},\boldsymbol{r}'} J_{\boldsymbol{r}\boldsymbol{r}'}\boldsymbol{S}_{\boldsymbol{r}}\cdot\boldsymbol{S}_{\boldsymbol{r}'} - \sum_{\boldsymbol{r},\boldsymbol{r}'} D_{\boldsymbol{r}\boldsymbol{r}'}(\boldsymbol{S}_{\boldsymbol{r}}\times\boldsymbol{S}_{\boldsymbol{r}'})\cdot\boldsymbol{n}_{\boldsymbol{r}\boldsymbol{r}'}. \quad (1)$$

Variables $\mathbf{S}_{\mathbf{r}} = (S^x_{\mathbf{r}}, S^y_{\mathbf{r}}, S^z_{\mathbf{r}})$ are classical spins of unit length, $|\mathbf{S}_r| = 1$, arranged into a cubic lattice. The first and second terms describe the exchange and DM interaction between spins at sites $\boldsymbol{r}$ and $\boldsymbol{r}'$. Below we suppose coupling constants $J_{\boldsymbol{r}\boldsymbol{r}'} = J$ and $D_{\boldsymbol{r}\boldsymbol{r}'} = D$ to be nonzero only for the nearest-neighbor sites and zero otherwise. The summation on $\mathbf{r}$ is over sites of the cubic lattice spanned by vectors $\hat{\mathbf{x}}$, $\hat{\mathbf{y}}$, and $\hat{\mathbf{z}}$. A unit vector $\boldsymbol{n}_{\boldsymbol{r}\boldsymbol{r}'}$ is directed from $\boldsymbol{r}$ to $\boldsymbol{r}'$, a vector $\boldsymbol{r}'$ indexes a half of the nearest neighbors of $\mathbf{r}$, i.e., $\mathbf{r}' = \mathbf{r}+\hat{\mathbf{x}}, \mathbf{r}+\hat{\mathbf{y}}, \mathbf{r}+\hat{\mathbf{z}}$, and the lattice spacing is taken to be unity, $a = 1$.

The exchange term (with $J > 0$) favors ferromagnetic spin alignment while the DM interaction twists neighboring spins relative to each other. In the low-temperature phase spins are arranged into a spiral with a wave vector $\boldsymbol{k}$ with a magnitude proportional to D/J and a sense of rotations defined by the sign of the DM interaction, a right-handed spiral corresponds to a positive D in Eq. (1). The Hamiltonian $H_{\rm lat}$ supplemented in an applied magnetic field with Zeeman term is widely used for MC simulation in two- and three-dimensional chiral magnets [21,23,25–29].

To describe a doped material one has to add an impurity term to Eq. (1). A unit cell of a real helimagnet such as MnSi is rather complicated; it contains four Mn and four Si ions and the real microscopic Hamiltonian takes into account this structure [30–32]. In the spin lattice model several unit cells are combined into a block cell with a resulting block spin $\boldsymbol{S}_{\boldsymbol{r}}$ which enters the Hamiltonian (1). To keep the matter simple we consider two possible arrangements of impurities. In the first model we assume that an impurity ion is substituted in place of one of the Mn ions and this leads to a new effective impurity spin $\boldsymbol{S}^c_{\boldsymbol{r}}$ for a given block cell positioned at $\boldsymbol{r}$. We assume that the impurity spin can be treated in the framework of the lattice spin model as a new spin variable of unit length coupled with neighboring spins of the regular lattice by some modified exchange and DM coupling constants J' and D'. In principle, there can be a case when two doped spins occur at neighboring sites $\boldsymbol{r}$ and $\boldsymbol{r}'$. At low doping concentration ($x < 0.2$) such cases are every rare, and besides, rich-impurity samples that we do not consider here would mimic FeSi or CoSi which as known are not magnetic, hence in our model we put couplings J' and D' to zero for two neighboring impurity spins.

In the second model we leave regular spins at their sites and add impurities into interstitial positions, i.e. place them between sites of the regular lattice. We again assume that the impurity can be treated as a unit spin $\boldsymbol{S}^c_i$. The impurity spin is considered frozen in some random direction and coupled by random exchange couplings with its eight nearest-neighbor spins $\boldsymbol{S}_{\boldsymbol{r}}$ of the regular lattice. These couplings $J^c_{i\boldsymbol{r}}$ are chosen randomly from an interval [0, 1]. As a result the doping part of the Hamiltonian can be described by a term

$$H_{\rm imp} = -\sum_{i,\boldsymbol{r}(i)} J^c_{i\boldsymbol{r}}\,\boldsymbol{S}^c_i\cdot\boldsymbol{S}_{\boldsymbol{r}}, \quad (2)$$

where i indexes a summation over all impurity spins $\boldsymbol{S}^c_i$ and $\boldsymbol{r}(i)$ means a sum over eight nearest neighbors of the impurity spin.

Below we refer to the first and second models as model A and model B, respectively. The first can be formally described by the Hamiltonian $H_{\rm lat}$ in which the coupling constants $J_{\boldsymbol{r}\boldsymbol{r}'}$ and $D_{\boldsymbol{r}\boldsymbol{r}'}$ are modified according to whether two regular spins or a regular and an impurity spin are coupled. The second model is described by the Hamiltonian $H_{\rm lat} + H_{\rm imp}$. In the model B the dynamics of regular spins are affected by the random frozen spins disseminated over the lattice, which turns out to greatly affect the magnetic structure of the lattice spins.

MC simulations were carried out on a $L\times L\times L$ cubic lattice of size $L = 30$ with periodic boundary conditions using a standard single-site Metropolis algorithm. In calculations we hold the parameter $J = 1$ fixed, serving as a unit of temperature. We start simulation at high temperature well above the magnetic transition temperature and then gradually decrease the temperature by sufficiently small steps $\Delta T = 10^{-2}$. We use 10^6 MC steps per spin (MCS) to equilibrate the system and the next 10^6 MCS to gain statistics. The equilibrated spin configuration is used as the initial spin configuration for the next run at a lower temperature. After we find the full

temperature dependence of $C(T)$ we make several runs with different arrangements of impurities and then average over the impurity distribution. In most runs we use $n_d = 8$ impurity distributions; we checked that the increasing of n_d does not change the resulting behavior of $C(T)$.

Discussing the Vollhardt invariance below, we apply an external magnetic field B along the z axis; the corresponding term in the Hamiltonian is $H_m = -B\sum_r S_r^z$. We use a protocol in which the system is cooled in a constant magnetic field. Different schemes of simulation in magnetic field do not change the Vollhardt crossing point and are discussed by us in Ref. [29].

From the simulation we directly calculate average spin configurations $\langle \mathbf{S_r} \rangle$, and an energy density, $E(T) = \langle H \rangle / N$, $N = L^3$. The specific heat we find by two ways: from differentiation of the energy density $C = dE/dT$ and from energy fluctuations $C = N(\Delta E)^2/T^2$. The comparison of relevant results is discussed below.

To analyze various spin configurations $\langle \mathbf{S_r} \rangle$ we find Fourier components, $\langle \mathbf{S_q} \rangle = 1/N \sum_{\mathbf{r}} \langle \mathbf{S_r} \rangle e^{-i\mathbf{q}\cdot\mathbf{r}}$ and then Bragg intensity profiles $I(\mathbf{q}) \propto |\langle \mathbf{S_q} \rangle|^2$. Presenting $I(\boldsymbol{q})$ we set $2\pi/L$ as a unit length in the $\mathbf{q}$ space. A spin spiral with a wave vector $\mathbf{k}$, $\mathbf{S_r} = S_\perp[\mathbf{e}_1 \cos(\mathbf{k}\cdot\mathbf{r}) + \mathbf{e}_2 \sin(\mathbf{k}\cdot\mathbf{r})]$, is characterized by two separate peaks of the $I(\mathbf{q})$ at points $\boldsymbol{q} = \pm\mathbf{k}$. This and other spin structures are convenient to analyze with the help of a projected intensity, $I^*(\bar{\mathbf{q}}) = \sum_{q_z(q_y)} I(q_x, q_y, q_z)$, which shows the profile of $I(\mathbf{q})$ projected onto (q_x, q_y) or, respectively, onto the (q_x, q_z) plane. For a spin spiral the projected intensity is $I^*(\bar{\mathbf{q}}) = (S_\perp^2/2)(\delta_{\bar{\mathbf{q}},\bar{\mathbf{k}}} + \delta_{\bar{\mathbf{q}},-\bar{\mathbf{k}}})$, where two-dimensional vectors $\bar{\mathbf{q}}$, $\bar{\mathbf{k}}$ are projections of vectors $\mathbf{q}$, $\mathbf{k}$ onto the corresponding plane.

III. RESULTS AND DISCUSSION

A. Model A

To illustrate the dependence of the specific heat on the impurity concentration we start our discussion with results obtained for model A. We set a parameter of DM interaction $D = 0.75$. This value was used in our previous calculations in analysis of the specific heat in parent MnSi [28,29] and it gives a pitch length of a spin spiral approximately equal to $\ell = 10a$ in the $\hat{\mathbf{x}}$ direction. Coupling constants for an impurity spin with its neighbors were chosen in a phenomenological way to be $J' = 0.1$ and $D' = 0$. Such a choice is dictated by experimental findings [14] which indicate that a substitutional replacement of Mn with Fe or Co suppresses the helimagnetic order in MnSi; in other words, in terms of the effective model, Eq. (1), such a substitution deteriorates DM coupling between impurity and the regular spin. Comments about other values of J', D' will be provided below.

Figure 1 shows the evolution of the temperature dependence of the specific heat with increasing impurity concentration. Function $C(T)$ is obtained from the fluctuation of the thermodynamic temperature. In a doping range from $x = 0$ to $x \simeq 0.15$ the behavior of $C(T)$ is typical of parent magnet MnSi; it shows a sharp peak of the magnetic first-order transitions followed by a second broad maximum anomaly, usually referred to as a hump, which extends over a temperature range up to $1.5J$. With increasing doping, the first-order

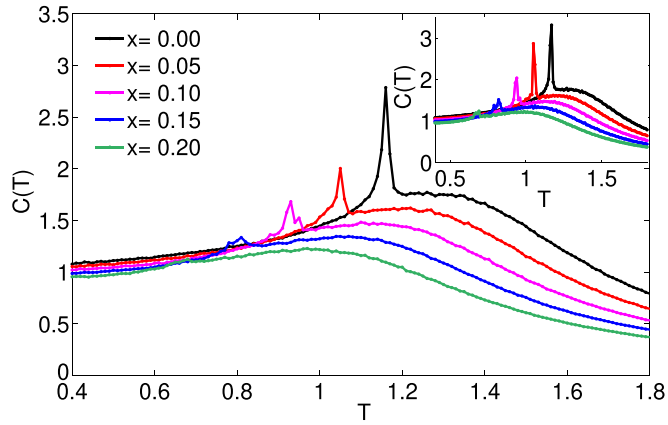

FIG. 1. Temperature dependence of the specific heat $C(T)$ for different doping concentration x for model A. Function $C(T)$ is obtained from fluctuation of the thermodynamic energy. The inset shows $C(T)$ obtained by differentiation of the thermodynamic energy.

peak shifts to lower temperature; it broadens and finally becomes degraded and disappears at $x \sim 0.2$. This resembles the experimental situation found in $Mn_{1-x}Fe_xSi$ [12–14]. In the same figure we also present for comparison the specific heat obtained from direct differentiation of the thermodynamic energy. Two $C(T)$ dependencies are similar to each other.

It is instructive to compare the evolution of $C(T)$ when one varies the parameter x with those obtained in an applied magnetic field B when one varies the magnitude of the field [29]; the two evolutions are different. Whereas in magnetic fields $B \lesssim 0.5$ the hump flattens out in such a way that the $C(T)$ curves for different B intersect with each other nearly at one point signaling the occurrence of the Vollhardt crossing phenomenon [33] and in fields $B \gtrsim 0.5$ the hump gradually starts to shift to higher temperatures; the variation of x leads to a quite opposite behavior: the maximum of the hump anomaly quickly diminishes and shifts to lower temperatures.

We also tested several other values of J' and D'. For magnitudes of J' in a range from 0.03 to 0.2 and D' lower than 0.1 we did not find substantial qualitative distinction in the resulting $C(T)$ curves. However, upon increasing the value of J' up to 0.5 and D' up to 0.2 we find that the sharp peaks of the specific heat persist and shift to lower temperatures in a wider range of doping concentrations, larger than $x \sim 0.2$. In our simplified model which treats an impurity as a simple substitution to a regular spin, lower values of J' and D' set a new scale for helical fluctuations, and do not considerably modify the nature of these fluctuations. This naturally leads to a lower scale for magnetic transition anomaly in the model under discussion.

As we showed above, the evolution of $C(T)$ curves with increasing doping concentration x does not show any signs of the Vollhardt crossing phenomenon. Next, we consider the combined effect of disorder and magnetic field. The main question we want to address is whether the Vollhardt invariance survives the disorder or not. In Fig. 2 we present results for the evolution of the specific heat in an applied magnetic field for disorder concentrations $x = 0.1$ and $x = 0.2$. The figures demonstrate the remarkable tendency of specific heat

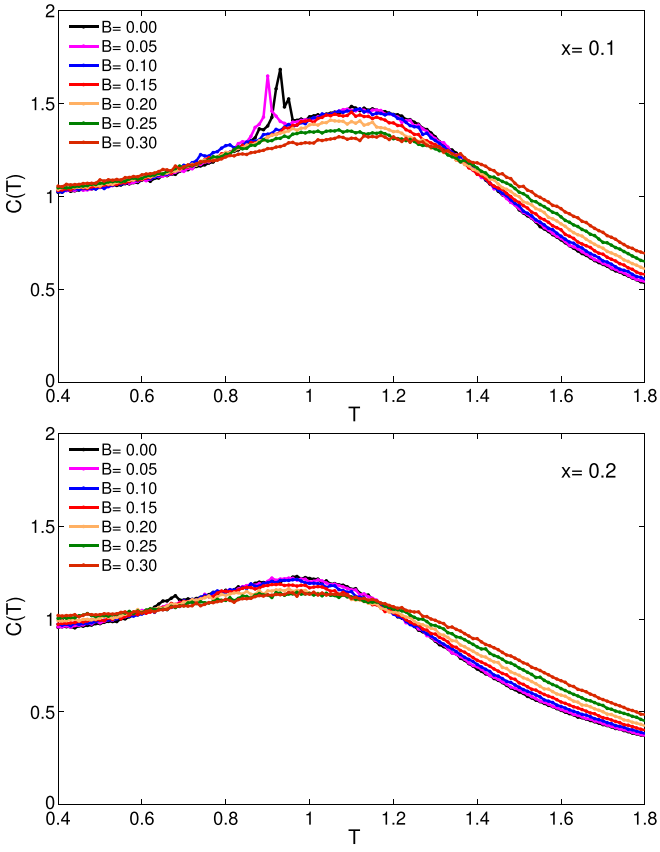

FIG. 2. Temperature dependence of the specific heat $C(T)$ in an applied magnetic field for doping concentration $x = 0.1$ and $x = 0.2$ for model A. Function $C(T)$ is obtained from fluctuation of the thermodynamic energy.

curves to cross at one or nearly at one point. The crossing point depends on the impurity concentration; the crossing point is $T^* \simeq 1.35$ for $x = 0.1$ and $T^* \simeq 1.15$ for $x = 0.2$. We note that the corresponding value of the crossing point without disorder is $T^* \simeq 1.4$ [29]. It shows that Vollhardt invariance survives intermediate disorder; the value of T^* gradually diminishes with x consistent with experimental results [14].

A remarkable difference in evolutions of $C(T)$ curves presented in Figs. 1 and 2 can be explained as the following. The main ingredient in the Vollhardt theory of the crossing phenomenon [33] is the the behavior of the entropy of the system $S(T, X)$ at different values of a controlling parameter X (in our case X is a magnitude of the magnetic field or a doping concentration). Crossing of the specific heat curves follows from a sum rule for the change of the entropy $S(T, X)$ with respect to X in the high-temperature limit [33]. In our system, the effect of disorder changes the entropy of the system in such a way that in the high-temperature limit the derivative $\frac{\partial S(T,x)}{\partial x} = \int_0^T \frac{dT'}{T'} \frac{\partial C(T',x)}{\partial x}$ depends on the amount x of the impurities introduced into the system. Such a behavior does not allow the occurrence of the crossing phenomenon.

Next we illustrate changes occurring in spin structure with doping. In Fig. 3 examples of spin configurations at different doping concentrations and temperatures are shown along with the corresponding Bragg intensity patterns. At low

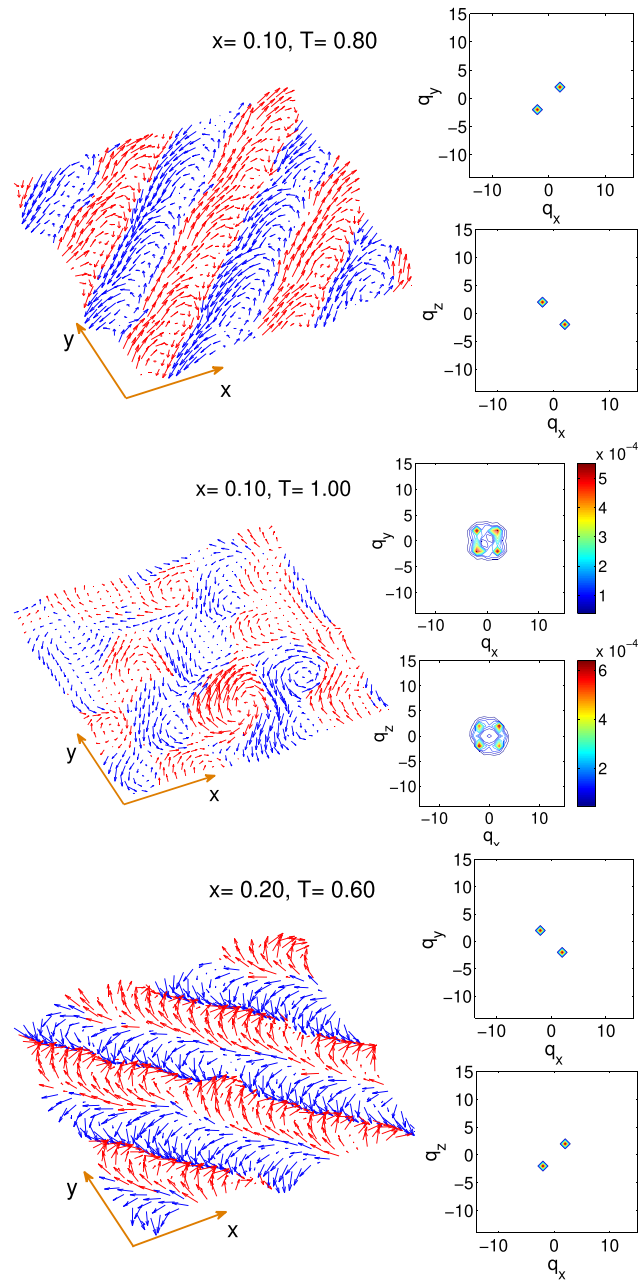

FIG. 3. Average spin configuration $\langle \boldsymbol{S}_{\boldsymbol{r}} \rangle$ in the xy plane (left) and profiles I^* of the Bragg intensity projected onto (q_x, q_y) and (q_x, q_z) planes (right) for model A. Spins with positive S^z are marked as red and negative S^z as blue. The length of the arrows is proportional to $|\langle \boldsymbol{S}_{\boldsymbol{r}} \rangle|$. Distances in the reciprocal space are scaled by $2\pi/L$.

temperatures spin patterns for all concentrations from $x = 0$ up to $x = 0.2$ are similar and have two peaks of Bragg intensity characteristic of a helical spin structure. However, the helical structure experiences small distortion with increasing x; this is seen from a pattern shown for concentration $x = 0.2$. The spiral shows irregular deviations from the direction of the spiral wave vector. With increasing temperature peaks of $I^*(\boldsymbol{q})$ begin to smear and at temperatures corresponding to the hump maximum, as illustrated for the concentration $x = 0.1$ at $T = 0.1$, the ring-shape profile of the $I(\boldsymbol{k})$ intensity is formed.

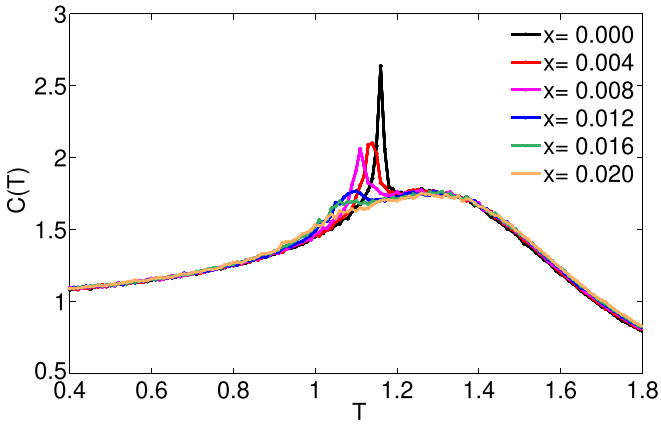

FIG. 4. Temperature dependence of the specific heat $C(T)$ for different doping concentration x for model B. Function $C(T)$ is obtained from fluctuation of the thermodynamic energy.

Such a pattern is seen at other impurity concentrations as well. The corresponding spin configurations consist of spin twirls typical of the chiral fluctuations in the hump region [11].

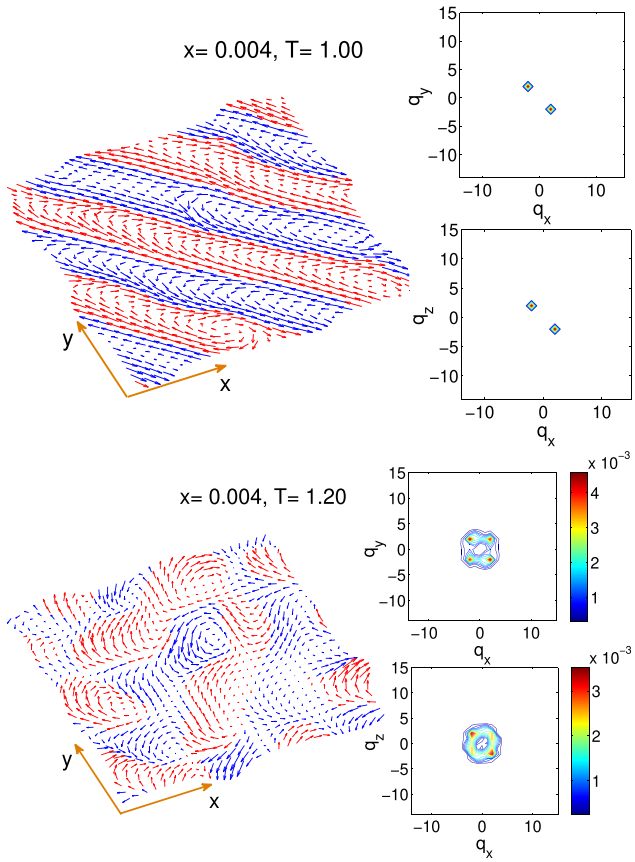

FIG. 5. Average spin configuration $\langle \boldsymbol{S}_{\boldsymbol{r}} \rangle$ in the xy plane (left) and profiles I^* of the Bragg intensity projected onto the (q_x, q_y) and (q_x, q_z) planes (right) for impurity concentration $x = 0.004$ for model B. Designations are the same as in Fig. 3.

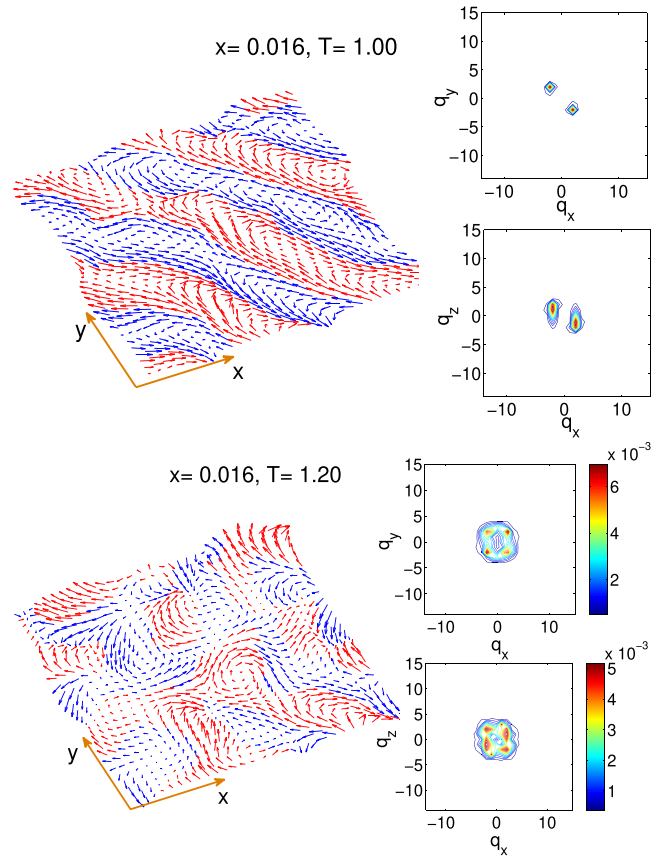

FIG. 6. Average spin configuration $\langle \boldsymbol{S}_{\boldsymbol{r}} \rangle$ in the xy plane (left) and profiles I^* of the Bragg intensity projected onto the (q_x, q_y) and (q_x, q_z) planes (right) for impurity concentration $x = 0.016$ for model B. Designations are the same as in Fig. 3.

B. Model B

The evolution of the specific heat for model B is presented in Fig. 4. Again, similar to model A, a sharp peak of a first-order transition gradually shifts to lower temperatures and smears away with increasing doping concentration. However, there are distinctions from model A. First, the degradation of the first-order peak occurs in the range of considerably lower concentrations of impurities, $x \lesssim 0.02$. It suggests that frozen random disorder is more efficient to suppress the magnetic transition than the dynamical impurity spins considered in model A.

The second distinction is that the shape and the maximum of the hump anomaly do not change appreciably with increasing x. It can be well understood taking into account that the frozen impurities do not have their own dynamics; as a result the redistribution of the energy upon heating takes place only amid regular lattice spins, and the hump is built up by the same helical spin fluctuations at different doping concentrations.

For illustration of Bragg intensity profiles we pick two temperatures. The first one, $T = 1.00$, corresponds to the low-temperature side of the hump, while the second, $T = 1.20$, lies almost at the hump maximum. The corresponding spin patterns are shown in Figs. 5 and 6. At $T = 1.00$ there are peaks of $I(\boldsymbol{q})$ corresponding to the spiral phase; these peaks are seen both at small, $x = 0.004$, and higher doping, $x =$

0.016. The spin pattern corresponds to a spiral. However, the structure of the spiral is different at low and higher x. At higher doping there are clear distortions from the perfect spiral structure; it resembles a "wavy" spiral with some small modulation of the spiral wave vector. In the spin pattern there are constrictions and wider parts in which small pieces of vortices appear. With increasing temperature there occurs a further distortion of the spiral phase; it is partitioned into disconnected segments, which start to form their own twirls, gradually going to a vortexlike pattern. Finally, at a higher temperature $T = 1.20$, at the hump maximum, one clearly sees the formation of the spin whirls with a Bragg intensity pattern typical of chiral fluctuations, namely, demonstrating a ringlike shape form of the intensity function $I(\boldsymbol{k})$ in $\boldsymbol{k}$ space.

Summarizing, with increasing impurity concentration there occurs a gradual distortion of the spiral phase. With increasing temperature the distorted spiral phase evolves continuously into a phase characterized by a spontaneous formation of the spin twirls and demonstrates a ring-shape structure of the Bragg intensity. This ring-shape structure is typical of the parent MnSi and does not change appreciably with doping.

IV. CONCLUSION

We have proposed two phenomenological models for a description of helimagnets with impurities. In the first one, impurities substitute the regular ions; in the second, the impurities reside in interstitial positions. In real materials two arrangements of doped impurities should take place simultaneously and the resulting specific heat dependence encompasses these two possibilities. Both models show a gradual suppression of the magnetic transition peak with increasing doping concentration. However, this suppression takes place on different scales of the concentration. While for model A the suppression takes place for values of x lower than 0.2, for model B it occurs for far less concentrations x, lower than 0.02. Also the evolution of the hump anomaly in the specific heat is different. While in model A the hump eventually shrinks to a smaller maximum and shifts to low temperatures, for model B its shape does not change appreciably in the considered doping interval.

We have analyzed the evolution of the spin structure emerging upon doping. In both models the low-temperature phase is a spiral phase. With increasing x the spiral pattern becomes significantly distorted by the presence of impurities, there occurs a gradual distortion of a helix rather than an abrupt destruction of the spiral phase. With increasing temperature the distorted spiral pattern continuously transforms into a vortexlike spin pattern similar to those seen in the region of the hump anomaly of the parent MnSi.

ACKNOWLEDGMENTS

This work was supported by the Russian Foundation for Basic Research (Grants No. 19-02-00509 and No. 18-02-00183) (A.M.B. and S.M.S.) and the Russian Science Foundation (Grant No. 17-12-01050P) (S.M.S.).

[1] A. E. Petrova and S. M. Stishov, J. Phys.: Condens. Matter **21**, 196001 (2009).
[2] S. M. Stishov and A. E. Petrova, Phys. Usp. **54**, 1117 (2011).
[3] S. M. Stishov, Phys. Usp. **59**, 866 (2016)
[4] S. M. Stishov and A. E. Petrova, Phys. Usp. **60**, 1268 (2017).
[5] M. Janoschek, M. Garst, A. Bauer, P. Krautscheid, R. Georgii, P. Böni, and C. Pfleiderer, Phys. Rev. B **87**, 134407 (2013).
[6] S. V. Grigoriev, S. V. Maleyev, A. I. Okorokov, Yu. O. Chetverikov, R. Georgii, P. Böni, D. Lamago, H. Eckerlebe, and K. Pranzas, Phys. Rev. B **72**, 134420 (2005).
[7] S. V. Grigoriev, S. V. Maleyev, E. V. Moskvin, V. A. Dyadkin, P. Fouquet, and H. Eckerlebe, Phys. Rev. B **81**, 144413 (2010).
[8] C. Pappas, E. Lelièvre-Berna, P. Falus, P. M. Bentley, E. Moskvin, S. Grigoriev, P. Fouquet, and B. Farago, Phys. Rev. Lett. **102**, 197202 (2009).
[9] L. J. Bannenberg, R. M. Dalgliesh, T. Wolf, F. Weber, and C. Pappas, Phys. Rev. B **98**, 184431 (2018).
[10] S. V. Grigoriev, N. M. Potapova, S.-A. Siegfried, V. A. Dyadkin, E. V. Moskvin, V. Dmitriev, D. Menzel, C. D. Dewhurst, D. Chernyshov, R. A. Sadykov, L. N. Fomicheva, and A. V. Tsvyashchenko, Phys. Rev. Lett. **110**, 207201 (2013).
[11] C. Pappas, A. O. Leonov, L. J. Bannenberg, P. Fouquet, T. Wolf, and F. Weber, Phys. Rev. Research **3**, 013019 (2021).
[12] J. Kindervater, T. Adams, A. Bauer, F. X. Haslbeck, A. Chacon, S. Mühlbauer, F. Jonietz, A. Neubauer, U. Gasser, G. Nagy, N. Martin, W. Häußler, R. Georgii, M. Garst, and C. Pfleiderer, Phys. Rev. B **101**, 104406 (2020).
[13] A. E. Petrova, S. Y. Gavrilkin, D. Menzel, and S. M. Stishov, Phys. Rev. B **100**, 094403 (2019).
[14] A. Bauer, A. Neubauer, C. Franz, W. Münzer, M. Garst, and C. Pfleiderer, Phys. Rev. B **82**, 064404 (2010).
[15] A. E. Petrova, S. Y. Gavrilkin, G. V. Rybalchenko, D. Menzel, I. P. Zibrov, and S. M. Stishov, Phys. Rev. B **103**, L180401 (2021).
[16] D. Belitz, T. R. Kirkpatrick, and T. Vojta, Phys. Rev. Lett. **82**, 4707 (1999).
[17] T. Vojta and R. Sknepnek, Phys. Rev. B **64**, 052404 (2001).
[18] J. Teyssier, E. Giannini, V. Guritanu, R. Viennois, D. van der Marel, A. Amato, and S. N. Gvasaliya, Phys. Rev. B **82**, 064417 (2010).
[19] S. Mühlbauer, B. Binz, F. Jonietz, C. Pfleiderer, A. Rosch, A. Nebauer, R. Georgii, and P. Böni, Science **323**, 915 (2009).
[20] S. V. Isakov, J. M. Hopkinson, and H.-Y. Kee, Phys. Rev. B **78**, 014404 (2008).
[21] S. D. Yi, S. Onoda, N. Nagaosa, J. H. Han, Phys. Rev. B **80**, 054416 (2009).
[22] A. Hamann, D. Lamago, Th. Wolf, H. v. Löhneysen, and D. Reznik, Phys. Rev. Lett. **107**, 037207 (2011).
[23] S. Buhrandt and L. Fritz, Phys. Rev. B **88**, 195137 (2013).

[24] A. O. Leonov and M. Mostovoy, Nat. Commun. **6**, 8275 (2015).
[25] M. C. Ambrose and R. L. Stamp, New J. Phys. **15**, 053003 (2013).
[26] A. O. Leonov, T. L. Monchesky, N. Romming, A. Kubetzka, A. N. Bogdanov, and R. Wiesendanger, New J. Phys. **18**, 065003 (2016).
[27] P. Milde, D. Köhler, J. Seidel, L. M. Eng, A. Bauer, A. Chacon, J. Kindervater, S. Mühlbauer, C. Pfleiderer, S. Buhrandt, C. Schütte, and A. Rosch, Science **340**, 1076 (2013).
[28] A. M. Belemuk and S. M. Stishov, Phys. Rev. B **95**, 224433 (2017).
[29] A. M. Belemuk and S. M. Stishov, Phys. Rev. B **101**, 144426 (2020).
[30] O. Nakanishi, A. Yanase, A. Hasegawa, and M. Kataoka, Solid State Commun. **35**, 995 (1980).
[31] J. M. Hopkinson and H.-Y. Kee, Phys. Rev. B **79**, 014421 (2009).
[32] V. A. Chizhikov and V. E. Dmitrienko, Phys. Rev. B **88**, 214402 (2013).
[33] D. Vollhardt, Phys. Rev. Lett. **78**, 1307 (1997).